

Structure and Dynamics of Propylene Oxide and Trimethylene Oxide Clathrate Hydrates

Inmaculada Peral,^{1,2} Joseph E. Curtis,¹ Bryan C. Chakoumakos,³ and Camille Y. Jones¹

¹NIST Center for Neutron Research, National Institute of Standards and Technology, Gaithersburg, MD 20899-8562 U.S.A. ²Department of Materials Science and Engineering, University of Maryland, College Park, MD 20742-2115 U.S.A. ³Condensed Matter Sciences Division, Oak Ridge National Laboratory, Oak Ridge, TN 37831 U.S.A.

ABSTRACT

We present results from studies of the structure and dynamics of clathrate hydrates of three cyclic ethers by neutron diffraction and preliminary results on molecular dynamics simulations. Recent results from neutron powder diffraction and quasielastic neutron scattering of studies of propylene oxide (PO, C₃H₆O) and its isomer trimethylene oxide (TMO, C₃H₆O), are compared with structural results obtained previously for tetrahydrofuran (THF, C₃H₅O). Experimental evidence of distortions of the host structures with temperature is discussed in light of the findings from quasielastic neutron scattering, which indicate distinct regions of high-temperature and low-temperature rotational dynamics and a temperature dependence related to the size of the guest. Preliminary MD results indicate a general expansion of the lattice with temperature resulting in increased volume available to PO.

INTRODUCTION

Clathrate hydrates [1] are inclusion compounds made of a hydrogen-bonded water "host" containing atoms or small molecules as "guests." The three-dimensional host network of spherical polyhedra of a clathrate hydrate (CH) is stable only when guest molecules are trapped within the polyhedra or cages. Restrictions on the size of a guest arise from the limited number of cage types that can encapsulate guest molecules while maintaining the necessary tetrahedral geometry for hydrogen bond formation. The guest-host (*g-h*) interactions are primarily repulsive, but for a guest with a permanent dipole, dipolar interactions may also be important and can affect, e.g., the rotational mobility of the guests [2] and the temperature at which the host H₂O molecules begin to rotate [3]. The nature of these interactions can be explored through a study of the changes in the crystal structures and rotational dynamics of the guests with temperature (*T*). Guest rotations in the range $10^6 < \nu < 10^{12} \text{ s}^{-1}$ are in the fast motion limit of NMR, but are within the dynamic range of neutron scattering.

In the present paper, we report results from neutron powder diffraction and quasielastic neutron scattering experiments on the CHs of three cyclic ethers, propylene oxide (PO, C₃H₆O) and its isomer trimethylene oxide (TMO, C₃H₆O), and tetrahydrofuran (THF, C₃H₅O), whose structures are shown in Fig. 1. The guest TMO forms clathrate hydrates with both the structure I (sI) and structure II (sII) frameworks (Fig. 2) depending on the composition of the initial mixture of TMO and water [4]. In each structure type, TMO occupies the large cage, i.e., the 5¹²6² cage in sI and the 5¹²6⁴ cage in sII (Fig. 2). Because of the differences in the shape, symmetry, and volume of the 5¹²6² and 5¹²6⁴ cages, TMO is expected to exhibit different behavior in each structure type. THF and PO are both larger than TMO and are only able to fit inside the 5¹²6⁴ cage in sII. All three molecules have permanent dipole moments. Molecular dynamics (MD)

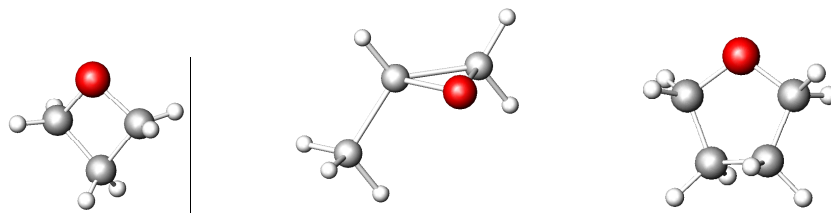


Figure 1. Molecular structures and van der Waals radii, r_{vdW} , for (left to right) TMO ($r_{vdW}=0.275$ nm), PO ($r_{vdW}=0.325$ nm), and THF ($r_{vdW}=0.30$ nm). The red, dark grey and light grey spheres represent O, C, and H atoms, respectively.

simulations were performed to simulate the temperature dependence of the unit cell volume for PO CH.

EXPERIMENTAL DETAILS

Sample preparation

To prepare sI TMO CH ($C_3H_6O \cdot 6.7^2H_2O$) and propylene oxide sII CH ($C_3H_6O \cdot 17^2H_2O$), with hydrogenated guest and deuterated host, stoichiometric amounts of the liquids were mixed in an atmosphere of He gas, poured into an 0.1-mm annular cylindrical aluminum can (20-mm o.d., 100 mm in height) and frozen inside an orange cryostat. The syntheses of sII THF CH ($C_4H_8O \cdot 17^2H_2O$) and sII TMO CH ($C_3H_6O \cdot 17^2H_2O$) is described elsewhere[5,6]. The sizes of the specimens to measure were chosen to scatter roughly 10% of the incident neutrons.

Measurements

Neutron powder diffraction. Measurements were made on the BT-1 32-detector neutron powder diffractometer at the NIST Center for Neutron Research [7]. The instrument was configured with a Ge(311) monochromator with a wavelength of 0.20787 nm, a take-off angle of 75° , and in-pile collimation of $15'$ of arc. The beam was masked to 1.59 x 5.08 cm at the sample. Data were collected over the range of $1.3^\circ < 2\theta < 161^\circ$ with a step size of $0.05^\circ 2\theta$.

Quasielastic Neutron Scattering. Measurements were performed on the Disk Chopper Spectrometer [8] with an incident wavelength of 0.48 nm resulting in an energy resolution of 0.120 meV full width at half maximum (FWHM). Neutrons were counted with 913 detectors spanning $-30^\circ < 2\theta < 120^\circ$. The neutron time-of-flight from the sample to the detector, t_{SD} , was measured in the range 1.5 ms to 10.5 ms, with a constant channel width of 0.009 ms and a neutron energy transfer range of -33 to 2.7 meV (energy loss).

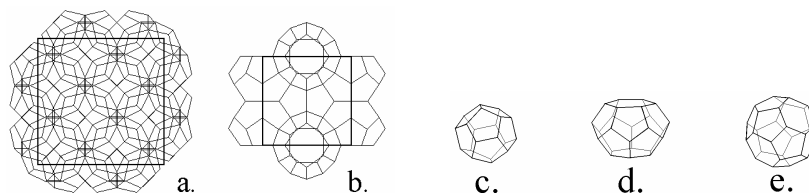


Figure 2. Structures of the cubic CHs: **a.** sII, **b.** sI; cage types in sI and sII CHs: **c.** 5^{12} , **d.** $5^{12}6^2$, **e.** $5^{12}6^4$. The notation 5^x6^y denotes a cage with x 5-sided faces and y 6-sided faces

Molecular Dynamics Simulation of sII PO CH

We utilized classical MD with empirical force-fields to simulate a fully-occupied sII PO CH crystal composed of eight unit cells in a periodic box. Simulations were performed using the CHARMM 27 force-field [9] incorporated into the program PINY_MD [10]. An SPC/E model was used for water [11]. PO molecules were parameterized using CHARMM atom types and short-range intermolecular interactions were modeled using the Lorentz-Berthelot mixing rule [12,13]. The initial configuration of sII PO CH crystal was chosen by using the experimentally determined coordinates of all PO atoms and CH oxygen atoms from structural data obtained 10 K. Initial coordinates for CH ^2H atoms were determined by a Monte Carlo procedure to minimize the overall net dipole of the system. Systems were equilibrated at each temperature for 500 ps; an additional trajectory of 600 ps was used for analysis.

RESULTS AND DISCUSSION

Neutron Powder Diffraction: Refinement of Data on sII PO CH

Refinement of data on sII PO CH. Rietveld refinement was performed with the General Structure Analysis System (GSAS) suite of programs [14] run through the interface program EXPGUI [15]. Refinements were performed on total intensity vs. 2θ . The crystal structure model for the sII host was taken from Jones et al. [5]. Lattice parameters, diffractometer zero point correction, profile parameters, and background were refined by the LeBail method [16]. Rietveld refinement of atom coordinates and U_{iso} was performed with a single $U_{\text{iso}}(\text{O})$ and $U_{\text{iso}}(^2\text{H})$. The PO molecule was treated as a rigid body. Cage volumes, V_{cage} , as defined by the O-atom positions [17] were computed with the program VINCI [18].

Variation of V_{cage} and V_{cell} with T . The variation of lattice parameters with T , plotted in Fig. 3a, for reflect a trend according to guest size, but similar temperature dependence. Cage volumes (Fig. 3b) for PO and THF CHs show a similar temperature dependence, with a contraction of the filled cage around 200 K. These results are in contrast to those of the $5^{12}6^4$ cages containing TMO, which increase smoothly with T , owing to the small size of this guest [6].

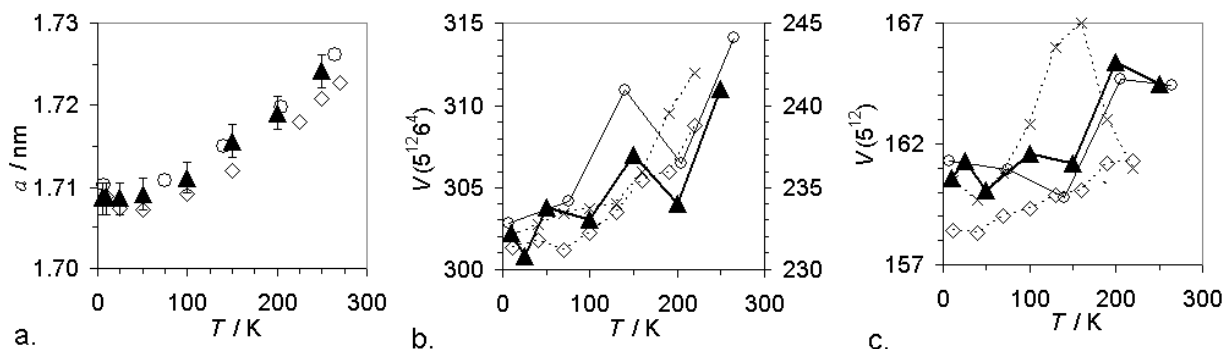


Figure 3. **a.** Lattice parameters as a function of temperature for sII CHs of PO (▲), sII TMO (◇), sI TMO (x), THF (○), and from MD simulation for PO sII CH (Δ). **b.** Temperature dependence of $V(5^{12}6^4)$ for sII PO, sII TMO, and sII THF, and $V(5^{12}6^2)$ for sI TMO; **c.** Temperature dependence of $V(5^{12})$ for PO, TMO, and THF CHs.

Quasielastic Neutron Scattering: A Comparison of sI TMO, sII TMO, and sII PO CHs

Data analysis. Data reduction and analysis were performed with the software suite DAVE [19]. At each temperature (T), data in the range $0.19 < Q < 2.36 \text{ \AA}^{-1}$ were grouped and converted to the double differential scattering cross sections, $S(Q, \omega)$, Fig. 4a, as described previously [20]. The intensity of the elastic peak in $S(Q, \omega)$ decreases with T and is accompanied by an increase in quasielastic broadening. The FWHM of the quasielastic components are independent of Q , therefore a simple reorientational process takes place over a restricted number of sites. The study of the temperature dependence of the FWHMs (Fig. 4b) suggest thermally-activated processes in two dynamical regions in temperature, below and above 50 K.

The integrated areas under the elastic and quasielastic portions of $S(Q, \omega)$ were used to calculate the experimental elastic incoherent structure factor or EISF [15]. The experimental EISFs are plotted in Fig. 5. All of the experimental EISFs display a minimum value (EISF_{\min}) and a corresponding value of Q (Q_{\min}) that decrease with T (Fig. 5). The shift of the minima of the curves to lower value of Q with increasing temperature indicates a change in the length scale of the motion at high T . The EISFs for sI TMO, sII TMO, and sII PO CHs indicate that the geometry of the motion is slightly different for the three guests.

Modeling the EISF. Fits to an isotropic diffusion model are unsatisfactory; a better fit is obtained if it is assumed that a fraction of the molecules undergo uniaxial rotations between two sites with unequal occupancy probabilities on a circle with radius r (\AA); for this case the EISF follows

$$\text{EISF} = f_1 + f_2 [p_1^2 + (1-p_1)^2 + 2p_1(1-p_1)j_0(Q \cdot r)] \quad (1)$$

where f_1 is the fraction of static molecules, and f_2 is the fraction of mobile molecules, p_1 is the occupancy probability of a site, and j_0 is the spherical Bessel function of the first order. This simplistic model does not consider the geometry of the molecule and the symmetry of the cage; however, a comparison of r and f_i for different guests at different temperatures is generally useful. The value of r obtained for sII TMO at 25 K and 35 K and sI TMO at 50 K is interpreted as the distance between the hydrogen atoms when the molecule rotates 90° about its C_{2v} axis. In general, motions above 50 K are more complex than uniaxial rotations. For example, above 50 K, the dynamics of sII TMO is better described by a model that accounts for the symmetry of the cage [13]. The increase in r with increasing T (Fig. 6a) may be an indication of translational freedom of the guest. The fraction of H atoms in motion in sI TMO, plotted in Fig. 6b, is

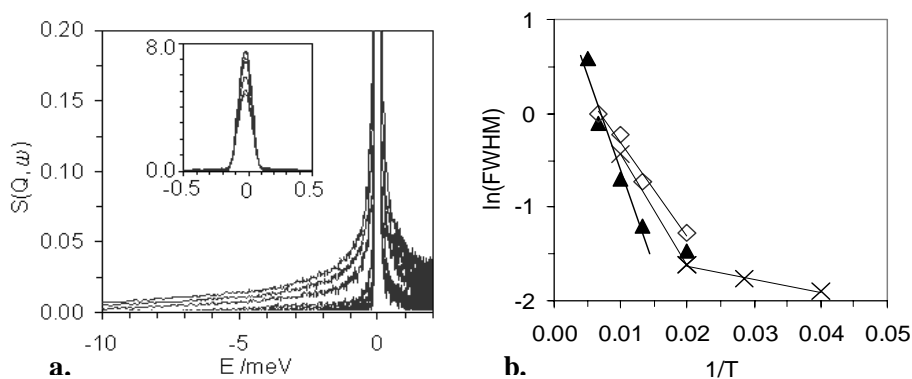


Figure 4. **a.** Corrected $S(Q, \omega)$ for sI TMO CH at (20, 35, 50, 75, 100, 150, 200, 225) K (bottom to top; top to bottom, inset). **b.** Plots of $\ln(\text{FWHM})$ versus $1/T$ for sI TMO (\diamond), sII TMO (\times), and sII PO (\blacktriangle) CHs.

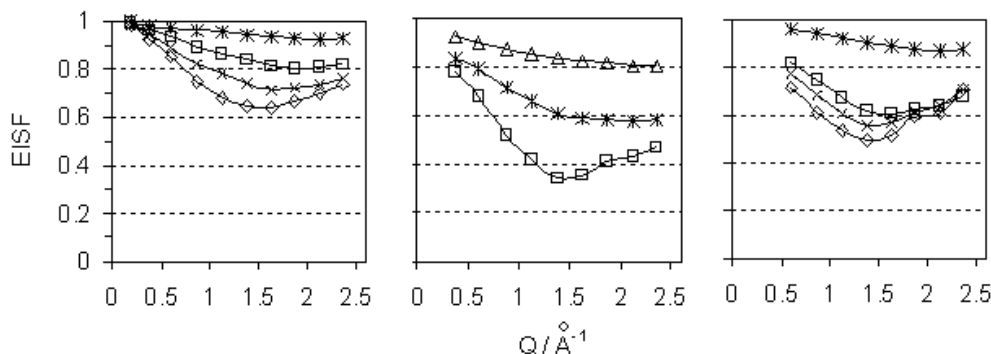


Figure 5. Experimental EISFs for (left to right) sI TMO, sII TMO, and sII PO CH at (top to bottom) 35 (Δ), 50 (*), 100 (\square), 150 (\times) and 200 K (\diamond).

significantly lower than that for sII TMO, which demonstrates that the dynamics of TMO in a sI CH is more restricted than in a sII CH. The fraction of H atoms in motion in a PO guest in a sII CH is lower than that of TMO in a sII CH, reflecting the larger size of PO.

Molecular Dynamics: Volume of the sII PO CH

Preliminary results predicted PO CH unit cell volumes (Fig. 7) systematically lower than the experimental values, with the difference decreasing with T (4.5 % at 10 K to 1.3 % at 200 K). Regardless, the simulations indicate a general expansion of the CH structure with T that accounts for the increased available volume to PO molecules which is in agreement with experiment. Hydrogen bonding was observed between PO and the CH host structure. We find that the hydrogen bond lifetime decreases with increasing T as expected, given the increased thermal energy of the system. The prediction of guest-host hydrogen bonding suggests that the choice of the initial configuration may effect the resulting structure and dynamics at each temperature. Alternative H_2O and PO models are being validated by comparison to QENS data.

ACKNOWLEDGMENTS

This work utilized facilities supported in part by the NSF under Agreement No. DMR-0086210. JEC acknowledges support from the NRC.

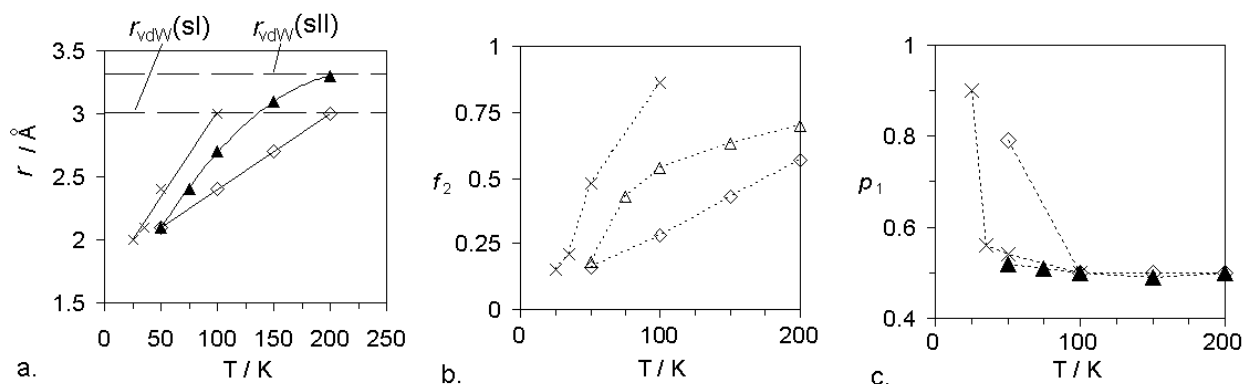


Figure 6. Plots of the fit parameters obtained with Eq. 1 versus T for sI TMO (\diamond), sII TMO (\times), and sII PO (\blacktriangle) CHs.

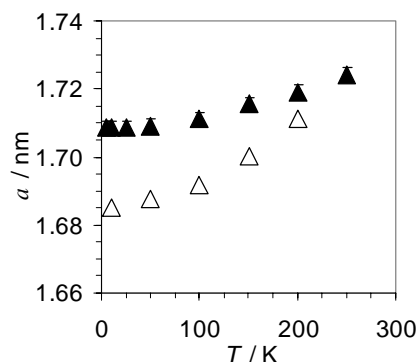


Figure 7. Comparison of the temperature dependence of experimental (▲) and MD (Δ) lattice parameters for sII PO CH.

REFERENCES

1. E.D. Sloan, Jr. "Clathrate Hydrates of the Natural Gases." Dekker: New York (1990).
2. S.R. Gough, *J. Phys. Chem.*, **77**, 2869 (1973).
3. J.A. Ripmeester, C. I. Ratliffe, "Inclusion Compounds Volume 5; Inorganic and Physical Aspects of Inclusion", eds. J. L. Atwood, J. E. D. Davies, and D. D. MacNicol (Oxford University Press, 1991) Chapter 2.
4. D. F. Sargent and L. D. Calvert, *Journal of Physical Chemistry*, **70**, 2689-2691 (1966).
5. C.Y. Jones, S.L. Marshall, B.C. Chakoumakos, C.J. Rawn, and Y. Ishii, *J. Phys. Chem. B*, **107**, 6026 (2003).
6. A. J. Rondinone, B. C. Chakoumakos, C. J. Rawn, Y. Ishii, *J. Phys. Chem. B* **107**, 6046 (2003).
7. The instrument is described at <http://www.ncnr.nist.gov/instruments/bt1>.
8. J. R. D. Copley and J. C. Cook, *J. Chem. Phys.*, **292**, 477-485 (2003).
9. A. D. MacKerell, Jr., D. Bashford, M. Bellott, R. L. Dunbrack Jr., J. D. Evanseck, M. J. Field, S. Fischer, J. Gao, H. Guo, S. Ha, D. Joseph-McCarthy, L. Kuchnir, K. Kuczera, F. T. K. Lau, C. Mattos, S. Michnick, T. Ngo, D. T. Nguyen, B. Prodhom, W. E. Reiher, III, B. Roux, M. Schlenkrich, J. C. Smith, R. Stote, J. Straub, M. Watanabe, J. Wiorkiewicz-Kuczera, D. Yin, M. Karplus, *J. Phys. Chem. B*, **102**, 3586 (1998).
10. M. E. Tuckerman, D. A. Yarne, S. O. Samuelson, A. L. Hughes, G. J. Martyna *Comp. Phys. Comm.* **128**, 333 (2000).
11. H. J. C. Berendsen, J. R. Grigera, and T. P. Stroatsma, *J. Phys. Chem.* **91**, 6269 (1987).
12. H. Lorentz, *A. Ann. Phys.* **12**, 127 (1881).
13. D. Berthelot, *C. r. Acad. Sci. Paris*, **126**, 1703 (1898).
14. A. C. Larson, R. B. Von Dreele, *General Structure Analysis System*, LAUR 86-748, Los Alamos National Laboratory.
15. B. H. Toby, *J. Appl. Cryst.* **34**, 210 (2001).
16. A. LeBail, H. Duroy, J. L. Fourquet, *Mat. Res. Bull.* **23**, 447-452 (1988).
17. B. C. Chakoumakos, C. J. Rawn, A. J. Rondinone, L. A. Stern, S. Circone, S. H. Kirby, Y. Ishii, C. Y. Jones, B. H. Toby, *Can. J. Phys.* **1/2**, 183 (2003).
18. B. Büeler, A. Enge, and K. Fukuda, "Exact volume computation for polytopes: A practical study." In: G. Kalai and G.M. Ziegler, editors, "Polytopes - Combinatorics and Computation," DMV-Seminars Vol. 29, Birkhäuser Verlag, Basel 2000
19. Data Analysis and Visualization Environment, described at <http://www.ncnr.nist.gov/dave>.
20. C. Y. Jones and I. Peral, *Amer. Mineral.* **89**, 1176 (2004).